EVIDENCE FOR ASYMMETRIC INERTIAL INSTABILITY IN THE FIRE SATELLITE DATASET

Duane E. Stevens and Paul E. Ciesielski
Department of Atmospheric Science, Colorado State University, Fort Collins, CO 80523

1. Introduction

One of the main goals of the First ISCCP regional experiment (FIRE) as stated in the original research plan – 'is obtaining the basic knowledge to better interpret satellite images of clouds on regional and smaller scales'. In this paper an analysis of a mesoscale circulation phenomenon as observed in hourly FIRE satellite images is presented. Specifically, the phenomenon of interest appeared on satellite images as a group of propagating cloud wavelets located on the edge of a cirrus canopy on the anticylonic side of a strong, upper–level subtropical jet. These wavelets, which were observed between 1300 and 2200 GMT 25 February 1987, are seen most distinctly in the GOES-West infrared satellite picture at 1800 GMT (Fig. 1). *The purpose of this paper is to document that these wavelets were a manifestation of asymmetric inertial instability.* (In this context, asymmetric means that the unstable perturbations exhibit structure in the direction of the basic state flow). During their lifetime, the wavelets were located over the North American synoptic sounding network, so that the meteorological conditions surrounding their occurrence could be examined (Section 2). A particular emphasis of the analysis in Section 2 is on the jet streak in which the wavelets were imbedded. The characteristics of the wavelets are examined in Section 3 using hourly satellite imagery. In Section 4 we examine the hypothesis that inertial instability is the dynamical mechanism responsible for generating the observed cloud wavelets. To further substantiate this contention, the observed characteristics of the wavelets are compared to, and found to be consistent with, a theoretical model of inertial instability by Stevens and Ciesielski (1986; hereafter referred to as SC). Our conclusions are summarized in Section 5.

2. Meteorological conditions

The meteorological conditions associated with the evolution of the cloud wavelets shown in Fig. 1 were investigated over the western two-thirds of the United States using conventional sounding data. Due to the paucity of these observations only the gross features of the upper–level flow field have been captured in our analysis. This problem is compounded even further by missing data which occurred in the vicinity of the jet stream probably due to radiosonde tracking problems.

On February 23, 1987, a vigorous winter storm system began affecting the western United States. By the 24th, the system was nearly occluded with an intense surface low centered over Nevada. The upper level features were dominated by a large, positively tilted trough which extended from Saskatchewan, Canada into a cutoff low centered over Nevada. Over the next few days the system weakened, but began to reorganize and intensify over New Mexico early on the 26th as an upper–level short wave propagating through the trough moved into a position favorable for support of the surface wave.

The upper–level jet stream in which the wavelets were imbedded is of particular interest to this study. Fig. 2 (left–hand panel) shows the wind speed analysis at 250 mb for 1200 GMT 25 February. At this time the jet core had maximum winds of 100 ms^{-1} and was centered around 250 mb; below this level vertical shears of 40 ms^{-1} $(100\ mb)^{-1}$ were present. South of the jet axis, horizontal shears were 10 ms^{-1} $(100\ km)^{-1}$. It is in this region of strong anticyclonic shear that the cloud wavelets were observed. In the 12 hour period following 1200 GMT 25 February the maximum intensity of the jet remained approximately constant (Fig 2, right–hand panel), however the horizontal wind shear on the anticyclonic side of the jet core reduced significantly to 7 ms^{-1} $(100\ km)^{-1}$.

3. Characteristics of the cloud wavelets

The predominant large–scale features in the satellite image of Fig. 1 are the cloudiness associated with the surface low over New Mexico and the broad shield of mainly high and middle–level clouds extending from southwest of Mexico to over the central states. This latter feature, which is often referred to as a 'baroclinic cloud leaf', is associated with a rising, moist airstream within the subtropical jet. Weldon (1979) has noted that the sharp western boundary of the upper tropospheric cloud leaf often coincides closely with a wind speed maximum or with a zone of strong winds.

In the satellite images prior to 1300 GMT, the western edge of the cloud leaf was relatively sharp and unperturbed. At 1300 GMT the cloud leaf over Baja, California showed the first evidence of being perturbed. During the next three hours two distinct wavelets grew over this region and propagated northeastward parallel

to the jet core axis until they appear to dissipate around 1700 GMT. Contemporary, with the dissipation of these wavelets a second group began to form near the U.S.–Mexican border. By 1800 GMT three cloud wavelets are observed. These wavelets propagated in a similar fashion to those described above and can be tracked until they dissipated around 2200 GMT; no wavelets could be identified after this time.

By creating a loop of hourly satellite images for the 25th, we were able to track the position of individual wavelets from one hour to the next. Fig. 3 shows the hourly positions of one of these wavelets superimposed with the locations of the jet axis. Fig. 3 also depicts the orientation and size of the wavelet during its life cycle. The general shape of the wavelets was that of an ellipse with its major axis oriented parallel to the jet axis. The life cycle of these wavelets appeared to have a growth stage ($\sim$ 1 hour), a mature stage (2–3 hours) and a decay stage ($\sim$ 1 hour) in which their identification becomes increasingly difficult. During their mature stage the wavelets varied in size from 200–250 km (along their major axis) and 65–100 km (along their minor axis). In addition, it appears that the wavelets moved parallel to the jet axis, in groups of two or three, and at a distance about 50 km to its anticyclonic side. In their mature stage the average distance between the centers of adjacent wavelets was $\sim$ 400 km. Using this scale as the wavelength (L_x) of the wavelets and noting that their average speed of propagation (c) was $\sim$ 80 ms^{-1}, we arrive at a period (L_x/c) for the wavelets of 1.4 hours. The brightness temperature in the interior of the cloud canopy ranged from -44 to -52 °C. Based on these values and the observed temperatures from soundings taken in the vicinity of these clouds, it appears that the wavelets and cloud leaf were composed of ice particles with cloud tops around 250 mb.

4. Dynamical mechanism for perturbed flow

Although several dynamical mechanisms (gravity waves, barotropic instability and inertial instability) could be hypothesized as the cause for the perturbed flow described above, the following discussion examines the most likely one, that is, *inertial instability.*

In the general case of flow with horizontal and vertical shear, a necessary condition for inertial instability is $fP < 0$ somewhere in the fluid where P is the potential vorticity and f the Coriolis parameter. Figs. 4 (left–hand panel) shows the analysis of potential vorticity for three layers between 200 and 400 mbs at 1200 GMT on the 25th. Due to the large number of missing and bad wind observations in the vicinity of the jet, we elected to use the geostrophic wind in the evaluation of P. Height data, which is used in the computation of geostrophic wind, had much better spatial coverage than winds for the times under consideration. The key feature in the analysis of potential vorticity on the 25th is a region of negative potential vorticity over New Mexico extending southwestward to over Baja, California. The region of negative P is evident in all three layers but is most pronounced above 300 mb where the anticyclonic shear associated with the jet streak was strongest. An alternate view of the potential vorticity analyses is presented in Fig. 5 which shows its relationship to the geostrophic wind in a cross–section through the jet. At the time of this analysis, the core of the jet streak and the associated region of large negative P were located several hundred kilometers upstream of where this cross–section was taken. The 'X' in Fig. 5 shows the observed location of the wavelets at 1800 GMT. From the analyses presented in Figs. 4 and 5, we conclude that *the condition for inertial instability was satisfied in the region and over the time frame that the wavelets existed.* A second area of weak negative potential vorticity is evident over southeastern Texas; however, its existence is questionable due to our lack of confidence in the geostrophic winds over this area.

The only significant change in the potential vorticity analysis at 0000 GMT on the 26th (Fig. 4, right–hand panel) is that the area of negative P directly to the anticylonic side of the jet streak, which on the 26th was positioned over Kansas, no longer existed. This suggests that the mechanism responsible for generating the wavelets also resulted in the elimination of the region of negative P.

Since inertial instability appears to be a reasonable explanation for the appearance of the wavelets, we now compare their characteristics (as discussed in Section 3) with theoretical estimates for asymmetric inertial instability from SC. For a Bickley jet of 75 ms^{-1} and a half–width of 3° at latitude 45° N, SC found that asymmetric perturbations would propagate at $\sim$ 45 ms^{-1} with respect to the ground (or 30 ms^{-1} slower than the maximum wind). The observed wavelets propagated at an average speed of 80 ms^{-1} (or 25 ms^{-1} slower than the maximum wind). Using SC's estimates of growth rate for asymmetric perturbations in the present case results in an unstable e-folding time scale of 5.4 hours; the wavelets life cycle was between 4–5 hours. Finally, SC estimated that the length scale of the asymmetric perturbations in the direction of the jet axis ($L_x/2\pi$) is comparable to the width of the unstable region. For the observed wavelets this length scale is $\sim$ 70 km whereas the width of the region with $P < 0$ varied between 100–200 km in the 250–300 mb layer. Although we have no means of estimating the vertical depth of the perturbed flow from the observed data, SC found that asymmetric modes of instability are preferred over the symmetric one for vertical scales greater than 3 km.

5. Concluding remarks

From the analyses in the previous sections we hypothesise the following scenario of events. At 1200 GMT on the February 25th a strong jet streak imbedded within the subtropical jet current was observed over Baja, California. South of the jet streak was an area of negative potential vorticity associated with the strong anticylonic shear in this region. During the next twelve hours this jet streak moved along the front side of a deep upper-level trough over the western U.S. at an average speed of ~ 25 ms^{-1}. During this period asymmetric inertial instability developed in response to the negative potential vorticity. This instability was manifested in a series of mesoscale cloud wavelets which formed along the western edge of a cirrus canopy. These wavelets, which were observed in satellite images between 1300 GMT and 2200 GMT on the 25th, propagated parallel to the jet core at an average speed of 80 ms^{-1}. These unstable perturbations acted to mix the flow thereby reducing the horizontal shears until the region of negative potential vorticity was eliminated.

This paper has presented the hypothesis that the wave disturbances observed in the satellite pictures of 25 February 1987 were excited by inertial instability. The characteristics of the cloud wavelets tend to support this hypothesis through comparison between observations and the theoretical estimates of SC. Analysis of the potential vorticity fields has been used to provide further evidence of a dynamical source of the instability. The observations represent a positive verification of the theoretical and numerical prediction of asymmetric instability in SC.

One might reasonably question the relationship between these observations and the extensive work of Emanuel and collaborators (e.g., Emanuel, 1979; Emanuel, 1982). In these papers Emanuel treated neutral waves which manifested a balance between the destabilising influence of vertical shear and stabilising Newtonian dissipation. Perturbations with structure along the direction of the parallel jet were not considered. By contrast, the instability treated here results primarily from the horizontal shear. Nevertheless, the *effect* of the instability is similar to that assumed in more recent Emanuel papers, that is, regardless of the particular structural characteristics of the perturbations, inertial instability serves to mix the potential vorticity, thereby causing the modified flow to have non-negative potential vorticity.

Our ability to describe the detailed characteristics of the instability presented in this paper has been limited by the sparseness of direct observations. These deficiencies in the observational data base have left us with many interesting, but unanswered questions. (e.g., What is the vertical scale of the perturbed flow? Are the instabilities characterized by vertical motion?) *The most direct way to answer these and other relevant questions would be with an intensive field observational program such as FIRE Cirrus IFO (Starr, 1987).* An alternate approach, which we are currently pursuing, is to model these instabilities. To our knowledge, explicit calculation of inertial instabilities in a two-dimensionally sheared basic state has not been accomplished.

Finally, it may be noted that initial analyses in numerical models may contain regions of negative potential vorticity and spurious rapid growth of unstable perturbations. One approach, already suggested by Dunkerton (1983) for equatorial shear, is to increase the numerical dissipation in order to eliminate the instability. Perhaps a more representative initialisation procedure would include an inertial adjustment step in which fP was required to be non-negative at every point in the domain.

Acknowledgements

The authors wish to thank Kelly Dean and Dick Johnson for their valuable contributions to this work. This research was supported by the Presidential Young Investigator Award (NSF Grant ATM-8352205) to D. Stevens.

REFERENCES

Emanuel, K. A., 1979: Inertial instability and mesoscale convective systems. Part I: Linear theory of inertial instability in rotating viscous fluids. *J. Atmos. Sci.*, **36**, 2425–2499.

Emanuel, K. A., 1982: Inertial instability and mesoscale convective systems. Part II: Symmetric CISK in a baroclinic flow. *J. Atmos. Sci.*, **39**, 1080–1097.

Starr, D. O'C, 1987: A cirrus-cloud experiment: Intensive field observations planned for FIRE. *Bull. Amer. Meteor. Soc.*, **68**, 119-124.

Stevens, D. E., and P. E. Ciesielski, 1986: Inertial instability of horizontally sheared flow away from the equator. *J. Atmos. Sci.*, **43**, 2845–2856.

Weldon, R. B., 1979: Cloud patterns and upper air wind field. *Part IV, Satellite Training Course Notes.* [Available from Satellite Application Laboratory, NESDIS/NOAA, Washington, D.C., 20233, 80 pp.]

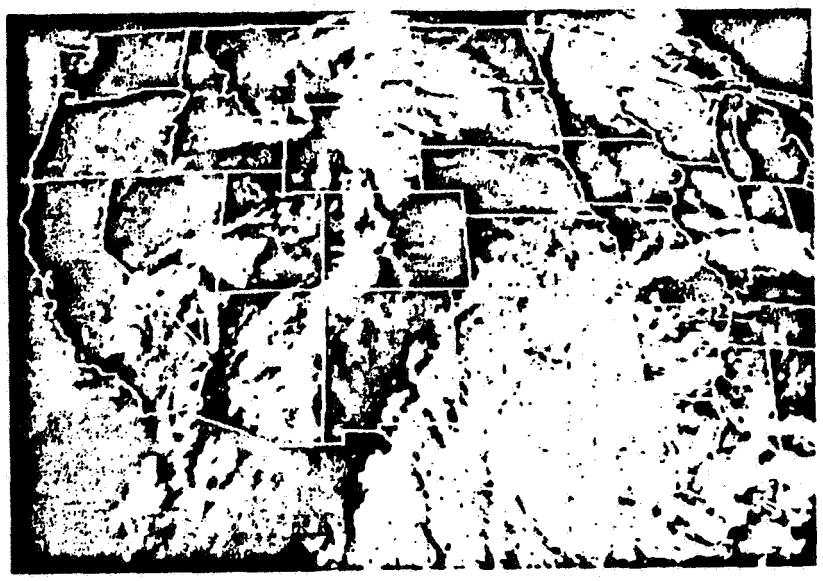

Figure 1. GOES-West infrared satellite image for 1800 GMT, 25 February 1987 showing mesoscale cloud wavelets over New Mexico.

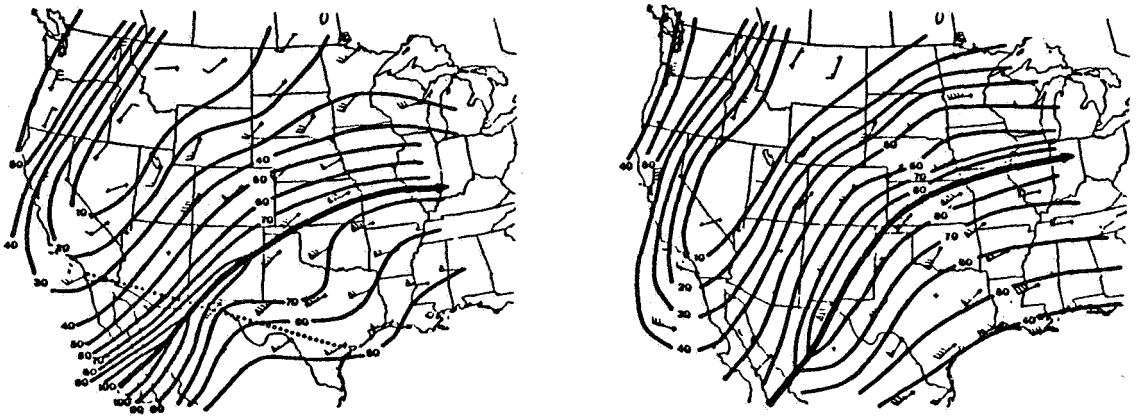

Figure 2. 250 mb wind speed analysis (ms^{-1}) at interval of 10 ms^{-1} for 1200 GMT, 25 February 1987 (left-hand panel) and 0000 GMT, 26 February (right-hand panel). Wind reports are from synoptic sounding network. Location of sounding stations is indicated by '+'; this symbol plotted without associated wind barb indicates that the wind data was missing. The jet stream axis is shown with a heavy solid arrow and wind speeds greater that 80 ms^{-1} are stippled. Dotted line shows projection for cross section in Fig. 5.

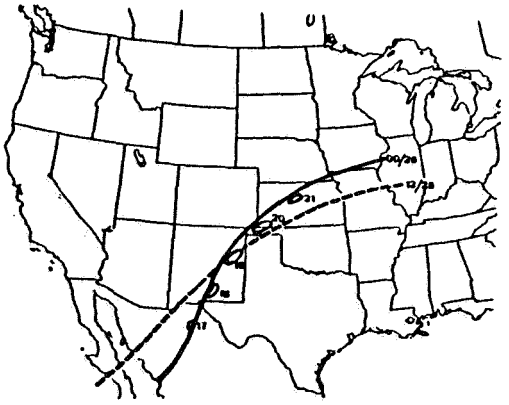

Figure 3. Hourly positions and shape of a single cloud wavelet inferred from satellite images. Numbers plotted by wavelet indicate the time (GMT) at which that position was observed. Also shown here are the positions of the jet stream axis at 1200 GMT, 25 February, 1987 (dashed line) and at 0000 GMT, 26 February, 1987 (solid line).

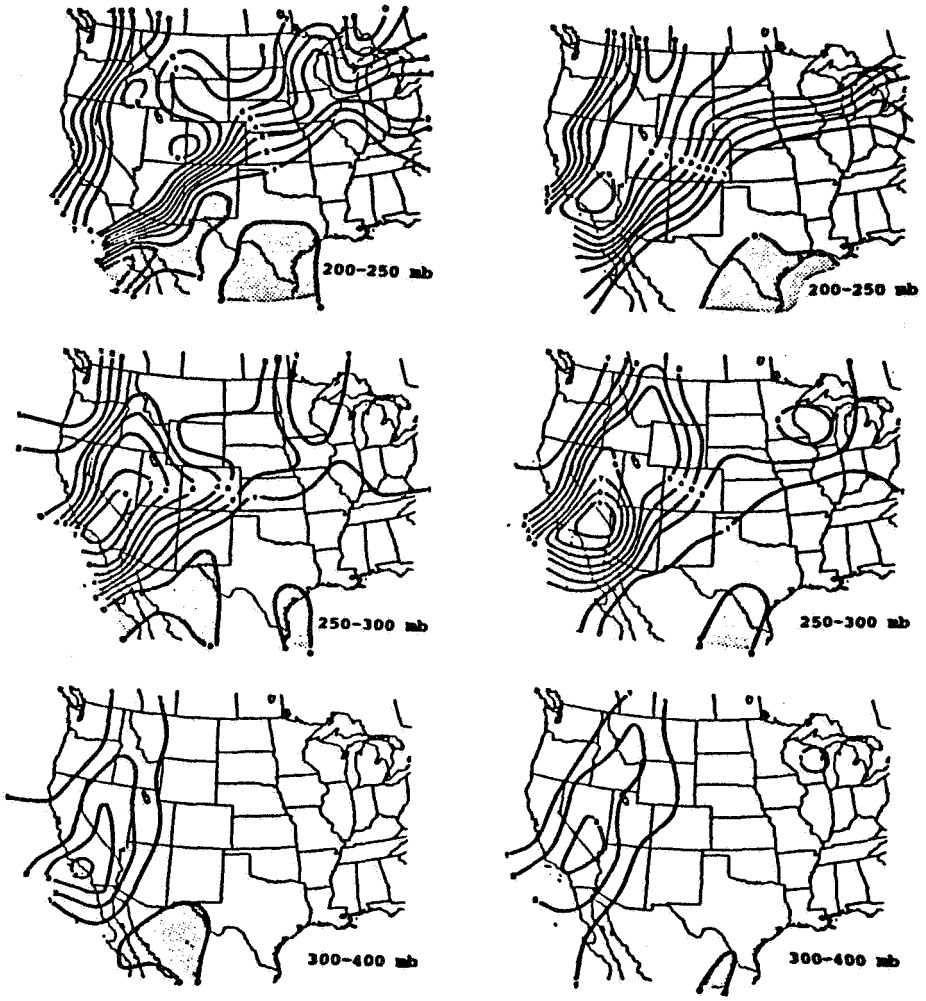

Figure 4. Analysis of potential vorticity ($m^2KKg^{-1}s^{-1}$) at 1200 GMT, 25 February 1987 (left-hand panel) and 0000 GMT, 26 February 1987 (right-hand panel) for the layers 200–250 mb (top), 250–300 mb (middle) and 300–400 mb (bottom). Values in figure have been multiplied by 10^6.

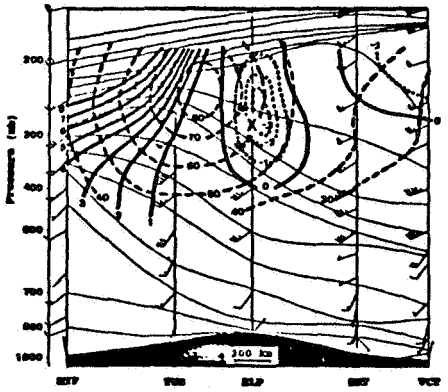

Figure 5. Cross-section analysis of geostrophic wind speed (ms^{-1}, heavy dashed lines) at intervals of 10 ms^{-1} and potential temperature (K, thin solid lines) at intervals of 5 K along dotted line in Fig. 2 for 1200 GMT, 25 February 1987. Plotted wind barbs show observed wind (ms^{-1}) for comparison to geostrophic wind speed. Analysis of potential vorticity ($m^2KKg^{-1}s^{-1}$, heavy solid line for positive values at intervals of 10^6 and dotted lines for negative values at intervals of 10^5). Position of wavelets at 1800 GMT on the 25th are denoted with an 'X'. Rawinsonde soundings are from San Diego, California (MYF), Tucson, Arizona (TUS), El Paso, Texas (ELP), Del Rio, Texas (DRT), Victoria, Texas (VCT).